Submitted to Magnetic Resonance in Medicine

FSL-MRS: An end-to-end spectroscopy analysis package

William T Clarke[a]*, Charlotte J Stagg[a], Saad Jbabdi[a].

a) Wellcome Centre for Integrative Neuroimaging, FMRIB, Nuffield Department of Clinical Neurosciences, University of Oxford, Oxford, United Kingdom.

* To whom correspondence should be addressed

Word count: 4710

Figure and table count: 6 figure & 3 tables

Running title: FSL-MRS

Keywords: Spectroscopy, MRS, MRSI, Bayesian fitting, open-source

Corresponding author contact details:

Dr William T. Clarke
Wellcome Centre for Integrative Neuroimaging, FMRIB
University of Oxford
Level 0
John Radcliffe Hospital
Oxford
OX3 9DU
UK

william.clarke@ndcn.ox.ac.uk

saad@fmrib.ox.ac.uk

Tel: 01865 610475

This manuscript has been submitted to Magnetic Resonance in Medicine.

Abstract

Purpose:

We introduce FSL-MRS, an end-to-end, modular, open-source magnetic resonance spectroscopy analysis toolbox. FSL-MRS provides spectroscopic data conversion, pre-processing, spectral simulation, fitting, quantitation and visualisation.

Theory and Methods:

FSL-MRS is modular. FSL-MRS programs operate on data in a standard format (NIfTI) capable of storing single voxel and multi-voxel spectroscopy, including spatial orientation information.

FSL-MRS includes tools for pre-processing of raw spectroscopy data, including coil-combination, frequency and phase alignment, and filtering. A density matrix simulation program is supplied for generation of basis spectra from simple text-based descriptions of pulse sequences.

Fitting is based on linear combination of basis spectra and implements Markov chain Monte Carlo optimisation for the estimation of the full posterior distribution of metabolite concentrations. Validation of the fitting is carried out on independently created simulated data, phantom data, and three in vivo human datasets (257 SVS and 8 MRSI datasets) at 3T and 7T.

Interactive HTML reports are automatically generated by processing and fitting stages of the toolbox. FSL-MRS can be used on the command line or interactively in the Python language.

Results:

Validation of the fitting shows low error in simulation (median error 11.9%) and in phantom (3.4%). Average correlation between a third-party toolbox (LCModel) and FSL-MRS was high (0.53-0.81) in all three in vivo datasets.

Conclusion:

FSL-MRS is designed to be flexible and extensible to new forms of spectroscopic acquisitions. Custom fitting models can be specified within the framework for dynamic or multi-voxel spectroscopy. FSL-MRS will be available as part of the FMRIB Software Library.

Introduction

Recent years have seen the emergence and rapid progress of new magnetic resonance spectroscopy (MRS) technologies, including spectral editing (1), MRS imaging (2,3), time-resolved functional MRS (4), diffusion-weighted MRS (5), and MRS fingerprinting (6). MRS is therefore starting to have a range of techniques comparable to those of conventional proton MRI, but with the added benefit of being able to quantify specific chemical compounds. However, unlike modern MRI-based neuroimaging, MRS lacks standard data formats (e.g. NIfTI (7)), as well as standard pre-processing and analysis pipelines suitable for use by non-expert users (e.g. FSL (8), SPM (9), or AFNI (10)). This restricts the use of MRS in research, particularly in neuroscience, by requiring expertise in MRS acquisition, data analysis, and computing. Current processing toolboxes are typically linear and linearly dependent, lacking modularity or a standardised data format. It is therefore difficult to customise processing pipelines, inspect the results of single steps of a pipeline, or combine steps from different toolsets.

The tools currently available and commonly in use for processing, fitting and visualisation of spectra (e.g. (11-16)) suffer from one or more of several limitations, namely:

- They may be black-box, closed-source implementations, sometimes with monetary cost.
- They may require licenced software to run, which is not universally deployable.
- They often require high user interaction, either through a GUI or the need for setting and understanding many options.
- They have fixed forward fitting models. Modifications require MRS and computing expertise.
- They have limited or no handling of MRSI data, with no parallelisation available.

For these reasons currently available software is not easily extensible to new forms of MRS, for example high-resolution, high-voxel count MRSI, or time-series modelling of functional MRS (fMRS), or diffusion-weighted MRS (dwMRS).

In this work we present a new Python-based MRS fitting and processing tool, FSL-MRS. The toolbox is open-source, free as part of the FSL software package (8), and operates with a scriptable command line or interactive interface. It implements a modular approach to spectroscopy analysis with a common data format, allowing integration with other neuroimaging tools. Steps are parallelisable for MRSI data. FSL-MRS is end-to-end, comprising modules for data conversion, pre-processing, basis spectra simulation, fitting, quantification, and visualisation.

The FSL-MRS fitting module works on the principle of linear combination of pre-calculated basis spectra (13). In keeping with FSL's tradition of favouring Bayesian inference approaches (17), our tool calculates full posterior distributions of the fitted metabolite concentrations using a Markov

chain Monte Carlo (MCMC) algorithm, specifically Metropolis-Hastings (18). The full posterior distributions can be utilised in further analysis, allowing efficient propagation of fitting uncertainties into downstream modelling and statistical analyses. Parameter covariances are also available from the fitting output, and point estimates of concentration and uncertainties may be calculated using appropriate summary statistics. FSL-MRS incorporates an interactive reporting interface which uses modern data-science visualisation tools.

In this work we describe the FSL-MRS components, interface and output, and describe the fitting model and approach. A validation of the tool's fitting estimates is carried out on widely available simulated data, in phantom and on three in vivo datasets at 3T and 7T, spanning 265 subjects.

Theory & Methods

Data conversion and format

FSL-MRS operates on a modular processing principle. Modularity allows custom third-party additions to the processing pipeline without the need to alter the FSL-MRS package or adhere to FSL-MRS imposed code conventions, languages, or possible limitations.

To enable this workflow FSL-MRS processing and fitting operates on MRS data stored in the Neuroimaging Informatics Technology Initiative (NIfTI) format (7). The NIfTI format permits the storage of data resolved into three spatial dimensions, in addition to a time dimension and two further unspecified dimensions. MRS and MRSI time-domain data may therefore be stored using the format (and it will also allow analysis of fMRS and dwMRS data in the future). Data is loaded from, and written to, file after each operation. Additional required meta-data is stored in, read from, and written to JavaScript Object Notation (JSON) "sidecar" files, as specified by the Brain Imaging Data Structure (BIDS) format (19).

FSL-MRS provides the spec2nii program to convert from existing data formats to NIfTI. Spec2nii currently supports seven formats specified in the supporting information (Supporting Table 1). Spectroscopy volume position information is translated into the NIfTI "qform" field where it is available in the original format.

Modular end-to-end processing

FSL-MRS provides a complete set of command line tools for spectroscopy analysis. Here we define *processing* as the steps required to make single voxel spectroscopy or reconstructed MRSI k-space data ready for *fitting*. *Basis spectra creation* is the process of using quantum mechanical simulations (or other methods) to create numerical descriptions of a metabolite's response to a specific MRS pulse-sequence. *Fitting* is the process of estimating relative metabolite concentrations from the processed spectrum and the basis spectra. *Quantification* turns those relative concentrations into

real-world interpretable units of concentration. *Display* incorporates viewing of the data and results at all stages of the process. Figure 1 shows an overview of the tool's workflow.

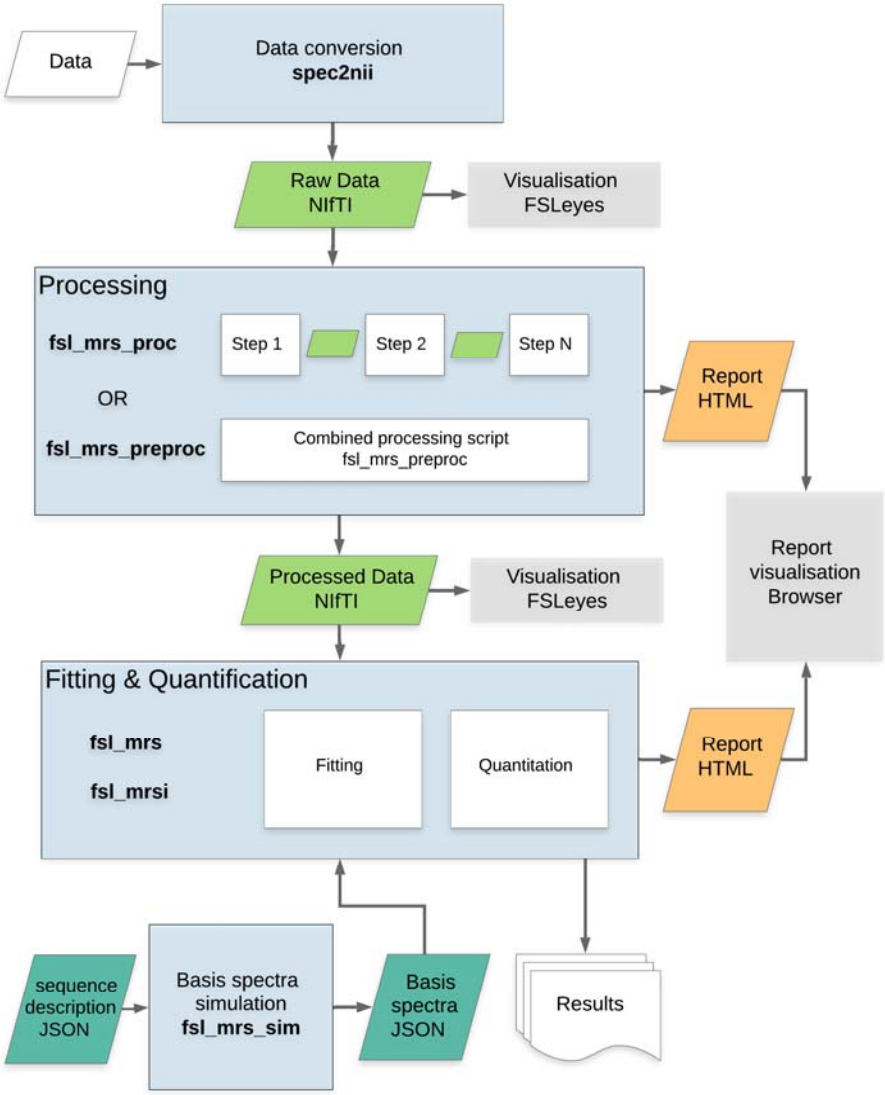

Figure 1 – FSL-MRS organisation and workflow. Raw data in proprietary or other formats are converted to NIfTI by spec2nii. Processing can then be carried out in stages, operating on NIfTI files, using fsl_mrs_proc, or in a single python script fsl_mrs_preproc for standard SVS sequences. Basis spectra can be generated for fitting using fsl_mrs_sim given a json description for the sequence. Fitting and quantitation are then carried out by fsl_mrs and fsl_mrsi as appropriate. Interactive HTML reports are generated for viewing in the user's browser. Spectroscopy data in NIfTI format can be viewed overlaid with other MR contrasts in FSLeyes.

Processing

FSL-MRS provides tools for all the processing operations recommended in the community-driven consensus paper (tables 2, 3 and 4 of reference (20)). These tools are accessed through the

command line by *fsl_mrs_proc* and are described briefly in Table 1. Coil combination is performed through the wSVD algorithm (21,22), spectral alignment by spectral registration (23), and nuisance peak removal by HLSVD (HLSVDPRO)(24). *fsl_mrs_proc* operations are applied sequentially to data stored in NIfTI format. Operations can be combined, in order, to form a repeatable batch processing script.

fsl_mrs_proc operation	**Description**	**Reference**
coilcombine	Combine individual coils of receiver phased array.	(21,22)
average	Average FIDs, with optional complex weighting.	
align	Phase and frequency align FIDs using spectral registration.	(23)
align-diff	Phase and frequency align sub-spectra based on addition or subtraction of sub-spectra (e.g. for ISIS localisation).	(23)
ecc	Eddy current correction using a water phase reference scan.	(25)
remove	Remove peak (typically residual water) using HLSVD.	(24)
tshift	shift/resample in time domain.	
truncate	Truncate/pad time-domain data by an integer number of points.	
apodize	Apply choice of apodizeation function to the data.	
fshift	Frequency domain shift.	
unlike	Identify outlier FIDs and remove based on similarity metric.	(14)
phase	Zero-order phase spectrum by phase of maximum point in range	
subtract	Subtract two FIDs	
add	Add two FIDs	

Table 1: Processing operations available using the fsl_mrs_proc command line tool

In addition to the flexibility offered by this script, FSL-MRS also provides a pre-packaged processing pipeline for non-edited single voxel data – *fsl_mrs_preproc*, which runs all appropriate steps with one command-line operation.

Basis spectra simulation

Fitting in FSL-MRS works on the principle of Linear Combination (LC) modelling (see Bayesian Fitting). LC modelling requires that the user provides the algorithm with simulated (or measured) numerical responses of metabolite spin systems to the MRS pulse sequence being used. These responses are specific to the pulse sequence, the sequence timings, and the sequence radio frequency (RF) pulse envelopes and are known as basis spectra. Basis spectra must preserve the relative signal amplitude between metabolites.

FSL-MRS provides an interface (*fsl_mrs_sim*) for the creation of basis spectra when provided with a description of the sequence timings, RF pulses, slice selection gradients and rephasing gradient areas. RF pulses may have arbitrary amplitude and phase modulation (i.e. be non-ideal). The

description is provided in a JSON format, examples are provided in the software documentation. The simulation is based on the extended 1D projection implementation of density matrix simulations (26). Unwanted coherences are removed with a coherence order filter (27). Standard literature values for common spin system chemical shifts and coupling constants are included in the software (28,29).

fsl_mrs_sim outputs a JSON file for each simulated metabolite which may be loaded by FSL-MRS's fitting modules. FSL-MRS also accepts LCModel (.BASIS) and jMRUI (.txt) basis spectra formats.

Fitting & Quantification

Fitting in FSL-MRS is provided by two command-line interfaces: *fsl_mrs* (for single voxel spectroscopy [SVS] data) and *fsl_mrsi* (for MRSI data). Additional interfaces will be added in the future for other types of MRS (e.g. diffusion-weighted MRS, functional MRS). Fitting is carried out on each voxel of data independently. The user may optionally specify: the limits of fitting (in ppm), the order of the complex polynomial baseline (see Standard fitting model), whether to add default macromolecular peaks (at 0.9, 1.2, 1.4, 1.7 and 2.08 & 3.0 ppm), the optimisation algorithm (see Optimisation). Metabolites in the basis spectra file may be optionally excluded by the user and, for output purposes only, metabolites may be combined.

For meaningful quantification the user must supply a processed unsuppressed water dataset, and for transverse relaxation-compensated concentrations the user must supply the sequence echo time and tissue volume fractions (30,31). The scripts *svs_segment* and *mrsi_segment* can calculate tissue volume fractions within each voxel given an appropriate T1-weighted structural image. Default values for water concentration, tissue-water densities, and water and metabolite T_2 time constants are provided for 3T and 7T field strengths. These defaults may be overridden in the interactive or python interface. Concentrations can be expressed as a ratio to an arbitrary internal reference metabolite (or combination of metabolites) or in molar (mol/dm^3) or molal (mol/kg) units.

FSL-MRS fitting outputs the signal-to-noise ratio (SNR) and linewidths (full width at half maximum) for each fitted metabolite. The SNR ratio is calculated as the ratio of the peak height of the fitted metabolite basis spectrum over the standard deviation of a pure noise region of the spectrum after a matched filter has been applied to both (32). The matched filter and linewidth are calculated for each metabolite as the FWHM peak width in hertz, as calculated from the most prominent peak in the fitted basis spectrum. If the MCMC algorithm is used the quality control metrics are calculated over all samples.

Reporting & Display

FSL-MRS modules generate self-contained interactive HTML reports (Plotly, Montreal, Canada) which can be viewed and interacted with in the user's web browser. All components of the processing module (Table 1) produce short HTML reports which can be combined into a single interactive report for each instance of data by using the packaged *merge_mrs_reports.*

An interactive report is generated for each fit displaying the fitted spectrum, model fit, residuals and concentrations (Fig 1) and concentration posterior distributions, metabolite covariances and scaled basis spectra (Fig 2). The user therefore can quickly assess the quality of SVS data and fit visually in one location. Results of the fitting are also available as comma-separated values (CSV) files from the command-line programs and as Pandas objects in memory (33).

Visualisation of both time and frequency domain MRSI data alongside structural imaging data can be achieved using the FSL package tool FSLeyes (34) (see Figure 3).

Interactive FSL-MRS

In addition to the command line tools described in the previous sub-section, FSL-MRS may be run in an "interactive" way by loading the underlying python libraries into an interactive IPython environment. The same functionality and reporting interfaces that are available on the command-line are also available interactively. In this way FSL-MRS allows prototyping of new processing pipelines and tools whilst also providing familiarity for users of interactive scripting languages.

Bayesian fitting

FSL-MRS implements linear combination modelling for fitting of basis spectra to data using Bayesian statistics to find an optimal solution. This method of fitting is robust whilst also outputting full posterior distributions of fitted metabolite concentrations to estimate concentration covariances and uncertainties.

The fitting module contains a standard fitting model appropriate for the fitting of a single independent spectrum. However, the fitting framework can accept an arbitrary forward model.

Standard fitting model

The model for the complex-domain spectrum is

$$\mathrm{Y}(\nu) = \mathrm{B}(\nu) + \exp[i(\phi_0 + \nu\phi_1)] \sum_{g=1}^{N_G} \sum_{l=1}^{N_g} C_{l,g}\, M_{l,g}\big(\nu; \gamma_g, \sigma_g, \epsilon_g\big) \#[1]$$

$$M_{l,g}\big(\nu; \gamma_g, \epsilon_g\big) = \mathcal{F}\big\{m_{l,g}(t) \exp\big[-\big((\gamma_g + \sigma_g^2 t) + i\epsilon_g\big)t\big]\big\} \#[2]$$

Where ν denotes frequency, $\mathrm{B}(\nu)$ describes an nth-order complex polynomial estimate of the baseline, the second term applies a global 0th and 1st order phase and the final term is the sum of all

scaled, shifted and broadened metabolite basis spectra $M_{l,g}(\nu; \gamma_g, \sigma_g, \epsilon_g)$. To avoid overfitting there is no flexibility in the metabolite line-shapes beyond shifting (ε) and broadening (γ, σ), which can be flexibly applied to N_G groups of metabolites (where each metabolite belongs to one and one only group). $\mathcal{F}$ is the Fourier transform and $m_{l,g}(t)$ is the inverse Fourier transform of $M_{l,g}(\nu; 0,0,0)$.

No prior information or constraints on relative metabolite scaling is incorporated.

Optimisation

Initialization is achieved using the truncated Newton algorithm as implemented in the SciPy package (35,36). The final fit is carried out over all model parameters using Metropolis-Hastings (a Markov Chain Monte Carlo algorithm) (18). The truncated Newton initialization can be used independently of the subsequent MCMC fit to provide a fast point-estimate of the metabolite concentration. In this work and in the summary reports generated by FSL-MRS, point-estimates of the metabolite concentrations from the MCMC algorithm are the arithmetic mean of the posterior distribution.

The forward model in Eq 1. is combined with an additive Gaussian white noise to produce the Likelihood function (which combines both real and imaginary part of the model prediction and data). The noise variance parameter is integrated out with a Jeffrey's (1/x) prior. Priors on the concentration parameters are set to broad zero-mean half-Gaussians (i.e. with positivity constraint). Line broadening parameters are set to broad Gaussians with a small positive centre (5Hz) and positivity constraints. Shift and phase priors are set to broad Gaussians centred at zero with no additional constraints. The baseline parameters are estimated in the initial nonlinear fitting then kept fixed in the MCMC stage.

Validation of fitting

All methods in this work refer to version 1.0.0 of FSL-MRS.

Simulation

Independently created simulated data was used to validate FSL-MRS. The simulated data was created by Malgorzata Marjanska, Dinesh Deelchand, and Roland Kreis for the ISMRM MRS Study Group's Fitting Challenge (37). The data comprises 21 datasets (without artefacts) with varying SNR, linewidths, line shapes, metabolite concentrations and macromolecule content. Briefly: datasets 0-2 have increasing widths of Lorentzian line-shapes; 3-5 have increasing widths of Gaussian line-shapes; 6-9 vary the concentration of GABA/GSH; 10 has no macromolecular content; 11-13, 14-16; 17-19, and 20 have different spectral SNR (20, 30, 40 & 160 respectively). The data simulates a 3T PRESS sequence with a T_E of 30 ms.

Both water-suppressed and unsuppressed data is provided in an already pre-processed state. Basis spectra for 20 metabolites, including a macromolecular baseline, were provided by the challenge

authors. True concentration values for each metabolite in each dataset were supplied by the Fitting Challenge authors in a private communication.

Fitting was assessed for both the Newton and MCMC algorithms. The polynomial baseline was restricted to 0th order and fitting was carried out between 0.2 and 4.2 ppm. After fitting, scaling of the raw metabolite concentrations was carried out using the unsuppressed water data, and concentration values were scaled accounting for provided tissue volume fractions (31).

Fitting performance was assessed using the mean and median percentage difference and absolute concentration difference from the true concentration values for each metabolite in all datasets. In addition, a summary statistic for each metabolite in each spectrum was calculated from the MCMC estimated posterior distribution as follows:

$$\frac{\mu_{[\mathrm{M}]} - [\mathrm{M}]_{\mathrm{True}}}{\sigma_{[\mathrm{M}]}}, \#[3]$$

where $\mu_{[M]}, \sigma_{[M]}$ are the mean and standard deviation of the fitted concentration of metabolite M and $[\mathrm{M}]_{\mathrm{True}}$ is its true value. Intuitively this statistic can be interpreted as "how many standard deviations away from the true value is our estimate".

Phantom

Validation of unsuppressed, water scaled concentrations was carried out in a uniform aqueous phantom (SPECTRE, Gold Standard Phantoms, London, UK) containing six metabolites (NAA, Cr, Cho, Ins, Glu and Lac) using a previously published STEAM sequence at 7T (38,39). The sequence parameters were: 11 ms TE, 32 ms mixing time (T_M), 10 s repetition time, 4096 samples, 6000 Hz bandwidth. Basis spectra were created using FSL-MRS, using a spatial resolution of 30 points in each dimension. The concentrations of six metabolites was determined from 5 Hz exponentially line-broadened spectra from the phantom. An additional doublet near 1.4 ppm was observed in the spectrum. It was established to be contaminant of the lactate feedstock used to create the phantom. It was fitted as alanine and included in the lactate concentration. Absolute concentrations were calculated from referencing the integral of the scaled creatine spectrum to an unsuppressed water spectrum taken to be equivalent to 55.5 M H_2O. T_2s were estimated from water and an average of metabolite singlet linewidths and concentrations were scaled for metabolite and water T_2 relaxation.

In vivo

FSL-MRS fitting was validated against LCModel (Version 6.3-1M) (13) in three in vivo datasets. The datasets covered different brain regions, sequences, and field strengths and are summarised in Table 2. Datasets one and two are single voxel sequences using STEAM and SPECIAL (40) sequences respectively and dataset three is 2D multi-voxel MRSI data collected using density-weighted

CONCEPT with a semi-LASER volume selection module (2). STEAM and SPECIAL data were processed using *fsl_mrs_proc* respectively.

All subjects in these datasets were recruited in a manner approved by the appropriate Research Ethics Committee for each originating study (see references in Table 2).

#	Sequence	B_0 (T)	Subjects	Voxels (brain regions)	Measured MM?	Vendor	Ref
1	STEAM	7	37	3 (ACC, OCC, putamen)	Yes	Siemens	(39)
2	SPECIAL	3	220	1 (PCC)	Yes	Siemens	(41)
3	CONCEPT	3	8	126 (calcarine sulcus)	No	Siemens	(42)

Table 2. Description of in vivo datasets used for validation. ACC = anterior cingulate cortex, OCC = occipital cortex, PCC = posterior cingulate cortex.

Identical basis spectra were used in both FSL-MRS and LCModel. Basis spectra for datasets one and two were created in FSL-MRS using fully described RF pulses, coherence filtering and with 30 spatial points in each dimension. The basis spectra comprised 19 and 17 simulated metabolites respectively to match previous analyses. Previously measured macromolecular spectra from metabolite-inversion-nulled sequences were included in the basis spectra. For dataset three existing basis spectra (as described in Ref (42)) were used. They were simulated in the simulation module of VeSPA (Versatile Simulation, Pulses and Analysis)(43) and comprise 19 simulated metabolites. Macromolecular spectra were not included; instead eight LCModel or FSL-MRS-simulated Gaussian macromolecule resonances were included in the analysis at the following positions: 0.91, 1.21, 1.43, 1.67, 1.95, 2.08, 2.25 and 3.00 ppm. For all datasets default “Concentration Ratio Priors” (also referred to as soft constraints) for metabolites were specified for the LCModel fit. The baseline flexibility parameter DKNTMN was set to 0.25, slightly above the default (0.15).

Datasets one and two were fitted using LCModel and FSL-MRS (MCMC algorithm). Dataset three was fitted in LCModel and FSL-MRS (Newton algorithm) for speed. Highly correlated peaks (correlation coefficient <-0.5) were combined (e.g. Cr+PCr, NAA+NAAG, PCh+GPC, Glu+Gln). Metabolite concentrations were expressed as a ratio to total creatine (Cr+PCr) and as molality concentrations using unsuppressed water as an internal reference. T_2 relaxation was accounted for, but the unsuppressed water peak was assumed to correspond to pure water as anatomical images for tissue segmentation were not available for all datasets.

Data was compared voxel-wise for each metabolite in each dataset using the Pearson correlation coefficient and Bland-Altman bias and limits of agreement (44). Bias is calculated as a percentage of the mean value, and the limits of agreement are the width of the 95% confidence intervals

expressed as a percentage of the mean value. In the comparisons, data was excluded if the estimated percentage Cramer Rao lower bounds on the metabolite concentrations exceeded 100% for either FSL-MRS or LCModel, or if the fitted value was more than four standard deviations from the mean value for that metabolite in that dataset. Metrics were calculated for both the water-scaled concentrations (water) and metabolite ratios (tCr); for all metabolites excluding the combined values (all) and for all metabolites including combined values but excluding those which were combined (combined).

Results

Output and reports

Figure 2 shows extracts of an example FSL-MRS fitting report. The extracts include a summary of the fit and metabolite concentrations, MCMC-estimated correlations between metabolite concentrations, and visualisations of the MCMC estimated distributions of the metabolite concentrations. Example fully interactive HTML reports for both fitting and processing are attached as supporting information. The same reports can be generated from example data included in the FSL-MRS package.

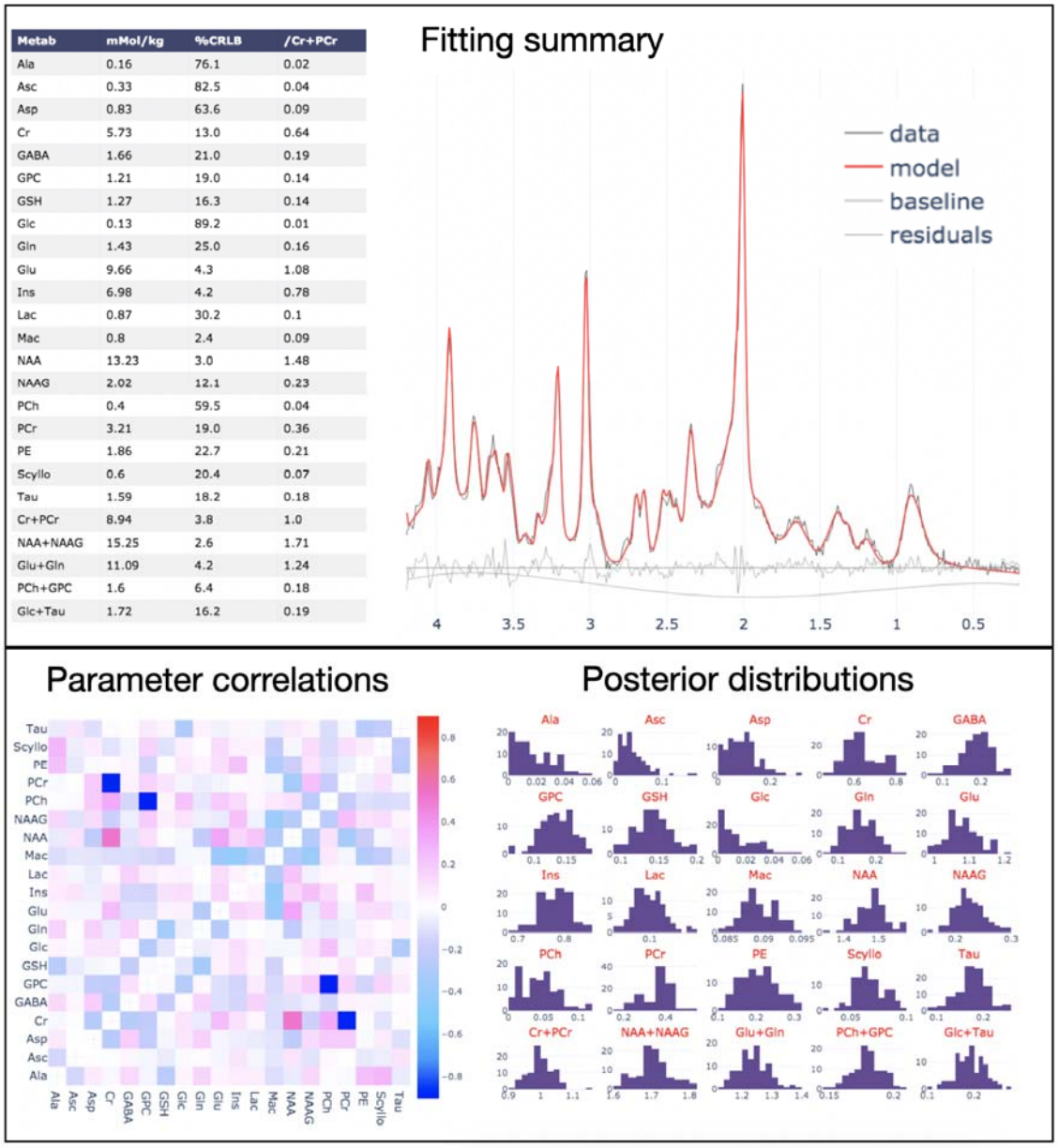

Metab	mMol/kg	%CRLB	/Cr+PCr
Ala	0.16	76.1	0.02
Asc	0.33	82.5	0.04
Asp	0.83	63.6	0.09
Cr	5.73	13.0	0.64
GABA	1.66	21.0	0.19
GPC	1.21	19.0	0.14
GSH	1.27	16.3	0.14
Glc	0.13	89.2	0.01
Gln	1.43	25.0	0.16
Glu	9.66	4.3	1.08
Ins	6.98	4.2	0.78
Lac	0.87	30.2	0.1
Mac	0.8	2.4	0.09
NAA	13.23	3.0	1.48
NAAG	2.02	12.1	0.23
PCh	0.4	59.5	0.04
PCr	3.21	19.0	0.36
PE	1.86	22.7	0.21
Scyllo	0.6	20.4	0.07
Tau	1.59	18.2	0.18
Cr+PCr	8.94	3.8	1.0
NAA+NAAG	15.25	2.6	1.71
Glu+Gln	11.09	4.2	1.24
PCh+GPC	1.6	6.4	0.18
Glc+Tau	1.72	16.2	0.19

Figure 2 – Extracts of the interactive HTML fitting report. **Top:** Metabolite concentrations summary and fit overlaid on data. Individual plots can be toggled on and off interactively. Bottom: correlations between metabolite concentrations from the Monte Carlo sampling (MCMC) and marginal posterior distributions of the metabolite concentrations. A full interactive fitting and pre-processing report is attached as supplementary information.

Figure 3 shows the results of fitting an MRSI grid of voxels from a single density weighted CONCEPT from dataset three (Table 2). NIfTI format viewers such as FSLeyes can be used to simultaneously view anatomical images, fitted metabolite concentrations, the spectral data and the FSL-MRS fit. In Figure 3 the total NAA concentrations are overlaid on a T1w image centred around the calcarine sulcus.

Fitting results may be exported in NIfTI or comma separated value (CSV) format or carried forward in python for further analysis.

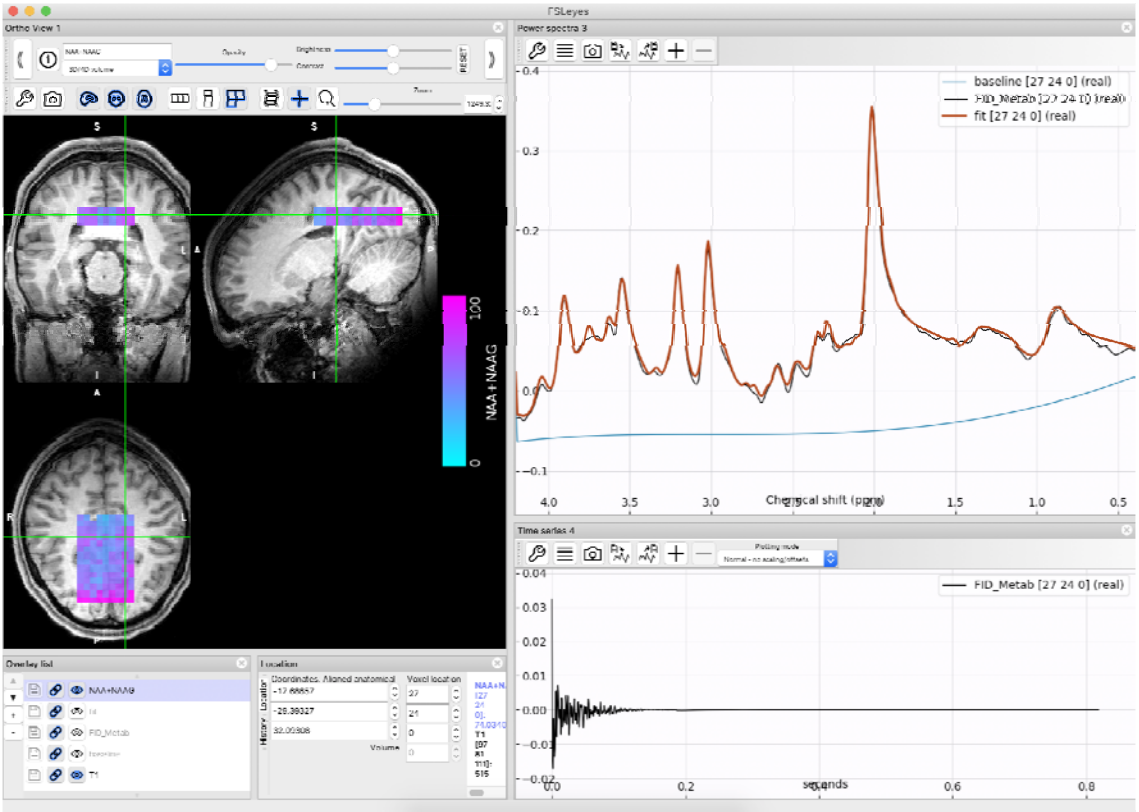

Figure 3 – MRSI in FSLeyes. The results of processing and fitting of MRSI data are stored in 4D NIFTI files and can be viewed in a suitable viewer such as FSLeyes. Here a map of total NAA (NAA+NAAG) as measured using CONCEPT (Dataset 3) is overlaid on a T1 weighted image. In the right-hand side panel the real part of the time series data for the selected voxel is seen on the bottom, and on the top the real part of the spectral data is overlaid with the FSL-MRS fit and baseline estimate.

Validation

Simulation

Figure 4 summarises the results of the validation on simulated data for all metabolites in all simulated datasets.

For all metabolites across all 21 datasets the Newton algorithm achieved a mean (median) absolute concentration difference of 0.60 (0.41) mM and a mean (median) absolute percentage difference of 30.6 (14.9) %. And for the MCMC algorithm 0.60 (0.37) mM and 35.2 (11.9) %. For the five most prominent signals (NAA+NAAG, Cr+PCr, Glu+Gln, Ins+Gly, GPC+PCho) the MCMC algorithm had a mean difference of 0.48 mM or 5.4%. The mean (±SD) number of standard deviations from the true value (Equation 3) was 0.57±0.43. 98.9% of true metabolite concentration values were between the 5th and 95th percentiles of the MCMC estimated posterior distributions. Uncombined choline (GPC &

PCh) and creatine (PCr&Cr) peaks were excluded from the calculation as described in the original fitting challenge results.

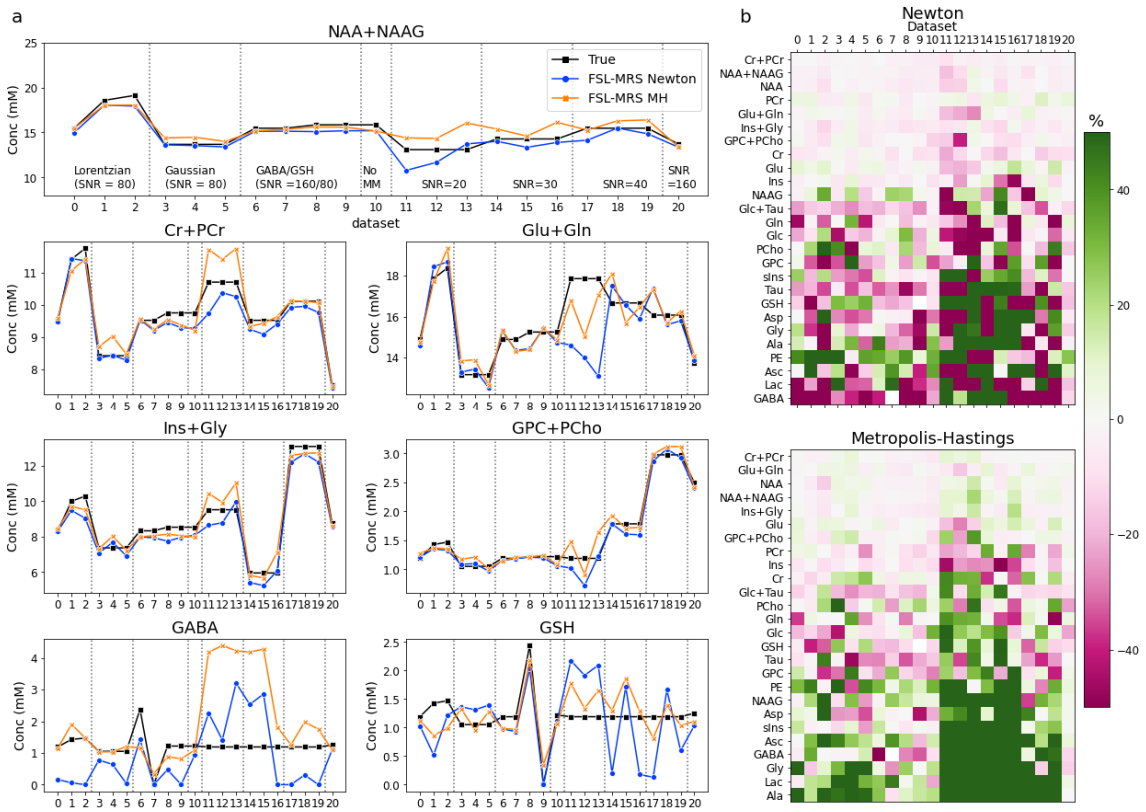

Figure 4 – Simulation validation. **a** Comparison of FSL-MRS measured concentrations for each MRS fitting challenge dataset for seven metabolites. **b** Percentage difference from true values for all metabolites for all datasets. The metabolites are sorted by mean difference. Both fitting algorithms (Newton [top] & Metropolis Hastings [bottom]) are shown.

Phantom

Figure 5 summarises the results of the absolute concentration validation in phantom. The mean absolute percentage difference from the true concentration across all metabolites was 3.39% (range -7.1% [Lac] to 1.1% [Glu]).

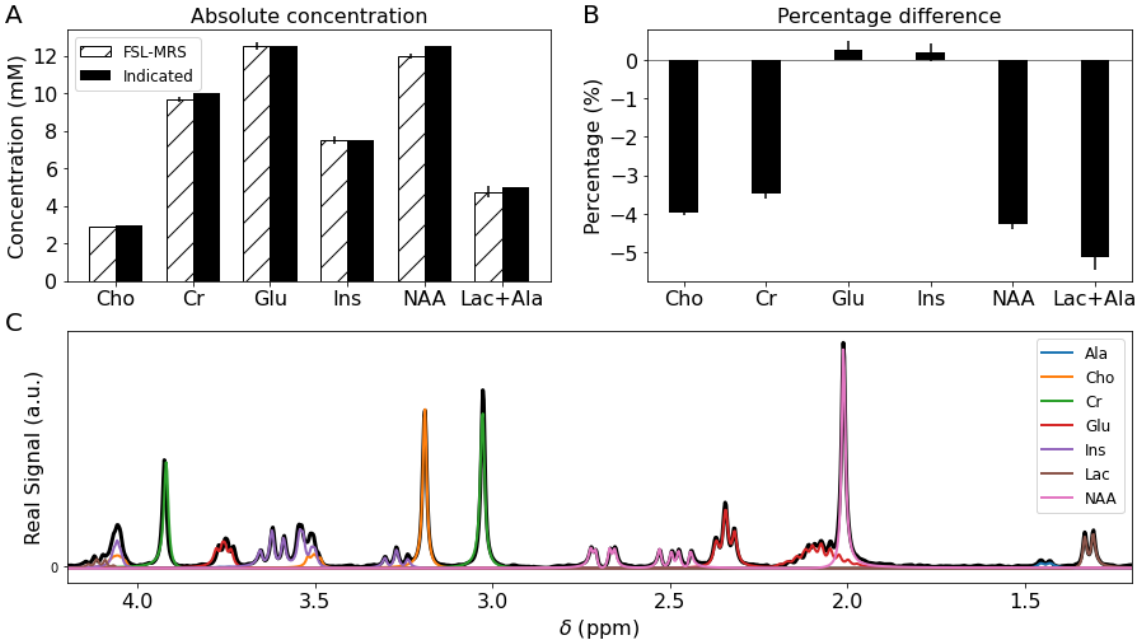

Figure 5 – Phantom validation. A) Absolute concentration of fitted metabolite compared to known concentrations. CRLB are indicated by vertical bars. B) Percentage difference from true value. C) Data overlaid with FSL-MRS fit, each metabolite fit is shown in a different colour. The doublet at 1.4 ppm is fitted as 'Ala' and included with lactate.

In vivo

Table 3 summarises the in vivo fitting validation correlations and Bland-Altman metrics for each dataset.

Mean correlations between FSL-MRS and LCModel in all data sets achieved a correlation over 0.5, and correlations were similar for both water-scaled concentrations and metabolite ratios. Correlations for the combined metabolite group were higher than the uncombined 'all' group, as the high SNR combined metabolites (Cr+PCr, PCh+GPC, Glu+Gln, NAA+NAAG, Ins) achieved correlations in the range 0.81 – 0.98 for all datasets. Figure 6 shows scatter plots for a sample of metabolites for each dataset. Concentrations and ratios were normalised to the maximum value fitted by either LCModel or FSL-MRS to facilitate plotting on the same axes. The scatter plots for all metabolites for each dataset are included as supplementary information (Supporting Figures S1-3).

Bland-Altman metrics showed a consistent bias for higher metabolite concentrations (mean of 14% to 37%) and metabolite ratios (11% to 24%) in FSL-MRS compared to LCModel. Bias was higher for water-scaled concentrations compared to metabolite ratios and lower for the combined metabolites.

Dataset	Scaling	Correlation *all*	Correlation *combined*	% Bias *all*	% Bias *combined*	% LoA *all*	% LoA *combined*
1) 7T STEAM	Water	0.69±0.18	0.74±0.19	22±21	14±12	120±71	93±64
	tCr	0.71±0.17	0.75±0.18	20±21	11±11	108±63	84±64
2) 3T SPECIAL	Water	0.68±0.13	0.75±0.12	44±25	45±27	414±329	369±345
	tCr	0.77±0.18	0.81±0.14	34±34	28±33	277±337	259±408
3) 3T CONCEPT	Water	0.53±0.16	0.56±0.14	37±22	37±20	216±109	193±92
	tCr	0.54±0.15	0.58±0.13	27±22	24±23	162±90	138±96

Table 3. Summary of in vivo validation – correlation and Bland-Altman statistics. *All = all metabolites (excluding combined), combined = after combination (excludes those combined), LoA = limits of agreement (width of 95% CI)*

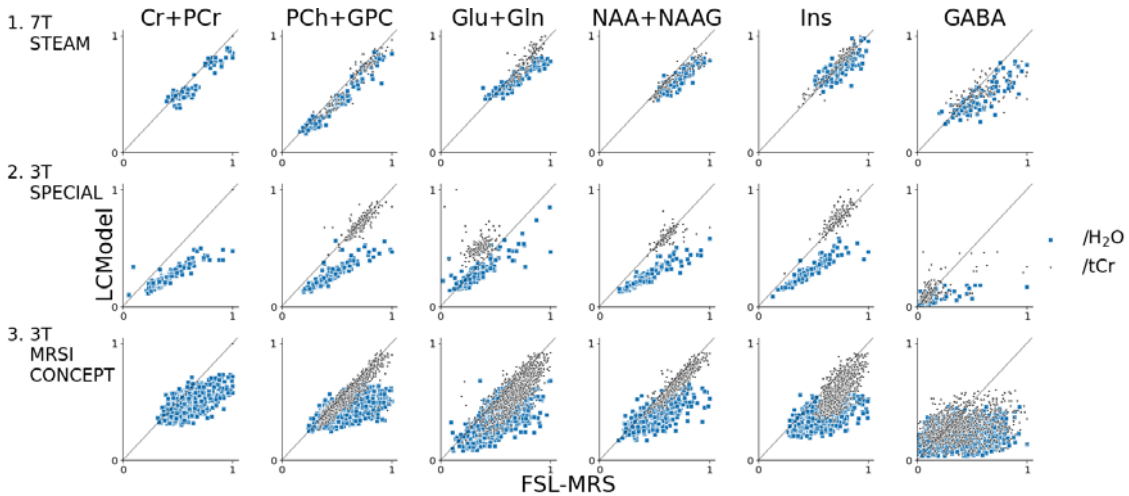

Figure 6 – Summary of *in vivo* validation. Correlation plots of a selected group of metabolites for each validation dataset. Ratios to unsuppressed water and total creatine (Cr+PCr) are normalised to the maximum value fitted by either FSL-MRS or LCModel are shown on the same axes. Correlation plots for all metabolites are shown in the supporting documents.

Discussion

FSL-MRS is an end-to-end spectroscopy analysis package. It is designed to be used flexibly: either implementing all stages of the MRS analysis pipeline or being used as a modular part of another pipeline. The package is scriptable on the command line requiring no interaction – suitable for analysis of large datasets and for deployment with high performance computing, or it can be used interactively – for pipeline prototyping and novel analyses.

It achieves modularity by operating on data stored in a standard file type, NIfTI, which is already in use throughout neuroimaging. Existing packages for handling NIfTI data exist in many programming languages (e.g. NiBabel in Python and the “image processing toolbox” in Matlab) enabling FSL-MRS

to be integrated with other MRS analysis programs. Results generated in NIfTI format allows straightforward integration of MRS data into multi-contrast analysis in existing neuroimaging toolboxes (e.g. FSL). Both FSL-MRS and Python are open source and free for academic and non-commercial use.

The package includes visualisation modules for generating interactive HTML reports viewable in a wide range of internet browsers. Visualisation of data and fitting results can also be accomplished in NIfTI format viewers due to the use of standard data types. Visualisation of data remains important whilst fully automatic quality control of MRS data remains not widespread (20).

Validation of the FSL-MRS fitting module was carried out on simulation, phantom and in vivo data. Validation on the simulated data showed low absolute concentration errors except in those datasets with low spectral SNRs (20 & 30) and in peaks with low SNR and high correlation with neighbours (e.g. GABA). Phantom validation indicated that the package correctly implements calculation of absolute concentrations using scaling to unsuppressed water in the case of pure water.

In in vivo data the validation was against LCModel, an established and widely used fitting program. Bias towards higher metabolite ratios in FSL-MRS was observed for water-scaled concentrations and, to a lesser extent, for relative metabolite ratios. The latter might arise from FSL-MRS not implementing priors between relative metabolite concentrations, a default setting in LCModel which was enabled in this analysis. Soft constraints in LCModel restrict certain metabolite concentration ratios (ratios of low SNR metabolites to a weighted average of NAA, total creatine and total choline) to be within a certain normally distributed range. The larger differences in water-scaled metabolite concentrations is likely due to the different implementations of flexible baselines in the two packages. Across all voxels in the MRSI dataset a high correlation was observed between absolute concentrations and the 0th order polynomial baseline parameter. A baseline below zero will increase the reference peak's absolute integral and result in a large ratio when compared with the integral of unsuppressed water. The effect of the precise implementation of flexible baselines on metabolite concentrations in fitting packages is complex (45,46) with dependence on acquisition, description of macromolecules in basis spectra and optimisation algorithm. FSL-MRS's implementation of a complex polynomial baseline does not offer a solution to this complexity, but the implementation is simple to understand and parametrised by 2n nuisance parameters for an order-n baseline. If enabled, the MCMC algorithm enables the user to calculate the covariance of the baseline parameters with the metabolite concentrations.

Fitting using the MCMC algorithm allows the user to generate the full posterior distribution for each fitted parameter, including metabolite concentrations. This information is essential to understanding

the uncertainties inherent in the estimation of the parameters. It also offers the opportunity to carry forward this information into subsequent study analysis, reducing the need for arbitrary quality cut-offs to be used. However, fitting using the MCMC algorithm is inherently slower than methods that only provide point estimates, taking 10s of seconds rather than seconds to compute the results for each voxel. It may be possible to achieve the estimation of the posterior distributions in the time frame of a few seconds using a variational inference optimiser, which is under development (47).

Operation of the package still requires the user to provide expert knowledge in two places: data conversion and generation of basis spectra. At the data conversion stage, the user must either use a file format understood by *spec2nii* and must interpret the structure of the data within that format, or provide a full conversion, including orientation information, for their own data format. Generating correct basis spectra requires the user to provide an accurate description of the RF pulses, timings and gradients in the localisation module of their sequence. Documentation for the package has been created to mitigate difficulties in these stages. *fsl_mrs* (SVS fitting) can interpret a select few other formats (LCModel ".RAW" & jMRUI ".txt").

The FSL-MRS MCMC fitting module accepts an arbitrary forward model. In future work we intend to use this framework to investigate the advantages of fitting multiple spectra simultaneously with a specialist model (e.g. for diffusion-weighted, edited or functional MRS).

Conclusion

We have presented a new end-to-end spectroscopy processing package incorporating Bayesian fitting of spectra. The package is open-source, modular and freely available. In this work validation of the package by simulation, in phantom and in three in vivo datasets has been provided. The complete package is available for download at git.fmrib.ox.ac.uk/fsl/fsl_mrs, through the open source package management system Conda (Continuum Analytics, Inc), and will be available as part of FSL (fsl.fmrib.ox.ac.uk).

Acknowledgements

Saad Jbabdi is funded by a Wellcome Trust Collaborative Award (215573/Z/19/Z).

Charlotte Stagg is supported by the Wellcome Trust and the Royal Society (102584/Z/13/Z).

The Wellcome Centre for Integrative Neuroimaging is supported by core funding from the Wellcome Trust (203139/Z/16/Z).

We thank Phil Cowen and Beata Godlewska for providing the STEAM data, collection of which was funded by the MRC [MR/K022202/1].

We thank Sana Suri, Enikő Zsoldos, and Klaus P. Ebmeier for providing data from the Whitehall II MRI substudy funded by the UK Medical Research Council (MRC) grant [G1001354; ClinicalTrials.gov Identifier: NCT03335696]. The research was also supported by the EU Horizon 2020 [Grant agreement number: 732592; "Lifebrain"] and the HDH Wills 1965 Charitable Trust [1117747].

We thank Aislin Sheldon, Holly Bridge and Jasleen Jolly for providing the MRSI validation data. This data was collected using funding from the MRC [MR/K014382/1], National Institute for Health Research (NIHR) [CA-CDRF-2016-02-002] and an MRC studentship.

We thank Malgorzata Marjanska, Dinesh Deelchand, and Roland Kreis for generating and providing the MRS Fitting challenge data.

We thank Sean Fitzgibbon, Michiel Cottaar and Paul McCarthy for providing their assistance and expertise in all matters Python.

We thank Jamie Near and Uzay Emir for useful discussions throughout the development of FSL-MRS.

References

1. Oeltzschner G, Saleh MG, Rimbault D, Mikkelsen M, Chan KL, Puts NAJ, Edden RAE. Advanced Hadamard-encoded editing of seven low-concentration brain metabolites: Principles of HERCULES. Neuroimage 2019;185:181-190.
2. Chiew M, Jiang W, Burns B, Larson P, Steel A, Jezzard P, Albert Thomas M, Emir UE. Density-weighted concentric rings k-space trajectory for (1) H magnetic resonance spectroscopic imaging at 7 T. NMR Biomed 2018;31(1).
3. Hingerl L, Strasser B, Moser P, Hangel G, Motyka S, Heckova E, Gruber S, Trattnig S, Bogner W. Clinical High-Resolution 3D-MR Spectroscopic Imaging of the Human Brain at 7 T. Invest Radiol 2020;55(4):239-248.
4. Ip IB, Berrington A, Hess AT, Parker AJ, Emir UE, Bridge H. Combined fMRI-MRS acquires simultaneous glutamate and BOLD-fMRI signals in the human brain. Neuroimage 2017;155:113-119.
5. Palombo M, Shemesh N, Ronen I, Valette J. Insights into brain microstructure from in vivo DW-MRS. Neuroimage 2018;182:97-116.
6. Kulpanovich A, Tal A. What is the optimal schedule for multiparametric MRS? A magnetic resonance fingerprinting perspective. NMR Biomed 2019:e4196.
7. NIFTI-1 Documentation. https://nifti.nimh.nih.gov/nifti-1/ (Accessed May 2020).
8. Jenkinson M, Beckmann CF, Behrens TE, Woolrich MW, Smith SM. Fsl. Neuroimage 2012;62(2):782-790.
9. Friston KJ. Statistical parametric mapping : the analysis of funtional brain images. Amsterdam ; Boston: Elsevier/Academic Press; 2007. vii, 647 p. p.
10. Cox RW. AFNI: software for analysis and visualization of functional magnetic resonance neuroimages. Comput Biomed Res 1996;29(3):162-173.
11. Deelchand DK. MRspa: Magnetic Resonance signal processing and analysis. Volume 2020. Minneapolis; Minnesota, U.S.A2020.
12. Edden RA, Puts NA, Harris AD, Barker PB, Evans CJ. Gannet: A batch-processing tool for the quantitative analysis of gamma-aminobutyric acid-edited MR spectroscopy spectra. J Magn Reson Imaging 2014;40(6):1445-1452.

13. Provencher SW. Estimation of metabolite concentrations from localized in vivo proton NMR spectra. Magn Reson Med 1993;30(6):672-679.
14. Simpson R, Devenyi GA, Jezzard P, Hennessy TJ, Near J. Advanced processing and simulation of MRS data using the FID appliance (FID-A)-An open source, MATLAB-based toolkit. Magn Reson Med 2017;77(1):23-33.
15. Wilson M, Reynolds G, Kauppinen RA, Arvanitis TN, Peet AC. A constrained least-squares approach to the automated quantitation of in vivo (1)H magnetic resonance spectroscopy data. Magn Reson Med 2011;65(1):1-12.
16. Stefan D, Di Cesare F, Andrasescu A, Popa E, Lazariev A, Vescovo E, Strbak O, Williams S, Starcuk Z, Cabanas M *et al.* Quantitation of magnetic resonance spectroscopy signals: the jMRUI software package. Meas Sci Technol 2009;20(10).
17. Woolrich MW, Jbabdi S, Patenaude B, Chappell M, Makni S, Behrens T, Beckmann C, Jenkinson M, Smith SM. Bayesian analysis of neuroimaging data in FSL. Neuroimage 2009;45(1 Suppl):S173-186.
18. Hastings WK. Monte-Carlo Sampling Methods Using Markov Chains and Their Applications. Biometrika 1970;57(1):97-&.
19. Gorgolewski KJ, Auer T, Calhoun VD, Craddock RC, Das S, Duff EP, Flandin G, Ghosh SS, Glatard T, Halchenko YO *et al.* The brain imaging data structure, a format for organizing and describing outputs of neuroimaging experiments. Sci Data 2016;3:160044.
20. Near J, Harris AD, Juchem C, Kreis R, Marjanska M, Oz G, Slotboom J, Wilson M, Gasparovic C. Preprocessing, analysis and quantification in single-voxel magnetic resonance spectroscopy: experts' consensus recommendations. NMR Biomed 2020:e4257.
21. Rodgers CT, Robson MD. Receive array magnetic resonance spectroscopy: Whitened singular value decomposition (WSVD) gives optimal Bayesian solution. Magn Reson Med 2010;63(4):881-891.
22. Rodgers CT, Robson MD. Coil combination for receive array spectroscopy: Are data-driven methods superior to methods using computed field maps? Magn Reson Med 2016;75(2):473-487.
23. Near J, Edden R, Evans CJ, Paquin R, Harris A, Jezzard P. Frequency and phase drift correction of magnetic resonance spectroscopy data by spectral registration in the time domain. Magn Reson Med 2015;73(1):44-50.
24. Laudadio T, Mastronardi N, Vanhamme L, Van Hecke P, Van Huffel S. Improved Lanczos algorithms for blackbox MRS data quantitation. J Magn Reson 2002;157(2):292-297.
25. Klose U. In vivo proton spectroscopy in presence of eddy currents. Magn Reson Med 1990;14(1):26-30.
26. Landheer K, Swanberg KM, Juchem C. Magnetic resonance Spectrum simulator (MARSS), a novel software package for fast and computationally efficient basis set simulation. NMR Biomed 2019:e4129.
27. Landheer K, Juchem C. Dephasing optimization through coherence order pathway selection (DOTCOPS) for improved crusher schemes in MR spectroscopy. Magn Reson Med 2019;81(4):2209-2222.
28. Govind V, Young K, Maudsley AA. Corrigendum: proton NMR chemical shifts and coupling constants for brain metabolites. Govindaraju V, Young K, Maudsley AA, NMR Biomed. 2000; 13: 129-153. NMR Biomed 2015;28(7):923-924.
29. Govindaraju V, Young K, Maudsley AA. Proton NMR chemical shifts and coupling constants for brain metabolites. NMR Biomed 2000;13(3):129-153.
30. Gasparovic C, Chen H, Mullins PG. Errors in (1) H-MRS estimates of brain metabolite concentrations caused by failing to take into account tissue-specific signal relaxation. NMR Biomed 2018;31(6):e3914.

31. Gasparovic C, Song T, Devier D, Bockholt HJ, Caprihan A, Mullins PG, Posse S, Jung RE, Morrison LA. Use of tissue water as a concentration reference for proton spectroscopic imaging. Magn Reson Med 2006;55(6):1219-1226.
32. Ernst RR, Bodenhausen G, Wokaun A. Principles of nuclear magnetic resonance in one and two dimensions. Oxford Oxfordshire, New York: Clarendon Press, Oxford University Press; 1987. xxiv, 610 p. p.
33. McKinney W. Data structures for statistical computing in python. 2010; Austin, TX. p 51-56.
34. McCarthy P. FSLeyes: zenodo; 2019. http://doi.org/10.5281/zenodo.3530921
35. Nash SG. Newton-Type Minimization Via the Lanczos Method. Siam J Numer Anal 1984;21(4):770-788.
36. Virtanen P, Gommers R, Oliphant TE, Haberland M, Reddy T, Cournapeau D, Burovski E, Peterson P, Weckesser W, Bright J *et al.* SciPy 1.0: fundamental algorithms for scientific computing in Python. Nat Methods 2020;17(3):261-272.
37. Marjanska M, Deelchand DK, Kreis R. MRS Fitting Challenge Phase 2. ismrm.org/workshops/Spectroscopy16/mrs_fitting_challenge/. The International Society for Magnetic Resonance in Medicine; 2016 (Accessed May 2020).
38. Emir UE, Auerbach EJ, Van De Moortele PF, Marjanska M, Ugurbil K, Terpstra M, Tkac I, Oz G. Regional neurochemical profiles in the human brain measured by (1)H MRS at 7 T using local B(1) shimming. NMR Biomed 2012;25(1):152-160.
39. Godlewska BR, Pike A, Sharpley AL, Ayton A, Park RJ, Cowen PJ, Emir UE. Brain glutamate in anorexia nervosa: a magnetic resonance spectroscopy case control study at 7 Tesla. Psychopharmacology (Berl) 2017;234(3):421-426.
40. Mekle R, Mlynarik V, Gambarota G, Hergt M, Krueger G, Gruetter R. MR spectroscopy of the human brain with enhanced signal intensity at ultrashort echo times on a clinical platform at 3T and 7T. Magn Reson Med 2009;61(6):1279-1285.
41. Suri S, Emir U, Stagg CJ, Near J, Mekle R, Schubert F, Zsoldos E, Mahmood A, Singh-Manoux A, Kivimaki M *et al.* Effect of age and the APOE gene on metabolite concentrations in the posterior cingulate cortex. Neuroimage 2017;152:509-516.
42. Steel A, Chiew M, Jezzard P, Voets NL, Plaha P, Thomas MA, Stagg CJ, Emir UE. Metabolite-cycled density-weighted concentric rings k-space trajectory (DW-CRT) enables high-resolution 1 H magnetic resonance spectroscopic imaging at 3-Tesla. Sci Rep 2018;8(1):7792.
43. Soher B, Semanchuk P, Todd D, Young K. Vespa: Integrated applications for RF pulse design, spectral simulation and MRS data analysis. 2011; Montreal. p 1410.
44. Bland JM, Altman DG. Statistical methods for assessing agreement between two methods of clinical measurement. Lancet 1986;1(8476):307-310.
45. Giapitzakis IA, Borbath T, Murali-Manohar S, Avdievich N, Henning A. Investigation of the influence of macromolecules and spline baseline in the fitting model of human brain spectra at 9.4T. Magn Reson Med 2019;81(2):746-758.
46. Marjanska M, Terpstra M. Influence of fitting approaches in LCModel on MRS quantification focusing on age-specific macromolecules and the spline baseline. NMR Biomed 2019:e4197.
47. Chappell MA, Groves AR, Whitcher B, Woolrich MW. Variational Bayesian Inference for a Nonlinear Forward Model. Ieee T Signal Proces 2009;57(1):223-236.